High-Cycle Fatigue response of MIM 8620 and 100Cr6 steels and their sensitivity to mean stress, notch sharpness and weld line position

Case-hardened MIM 8620 and hardened MIM 100Cr6 are two typical high-strength steel grades used widely for automotive applications produced by Metal Injection Moulding (MIM). In a comprehensive study by GKN Sinter Metals, the notch sensitivity of both these grades is investigated under both static and cyclic loading conditions. Of particular interest was the impact of weld lines – an often unavoidable feature of complex injection moulded components. What is the effect on a component's HCF response when weld lines are located in highly-loaded regions? Here, Dr.-Ing. Markus Schneider and colleagues present conclusions that will be of value to MIM producers and users alike.

Industrialised in the 1980s, the Metal Injection Moulding process allows industry to combine the high geometrical degree of design freedom offered by plastic injection moulding with the high strength properties of fully dense steels. Using the MIM process, which is divided into the injection moulding, debinding and sintering stages, it is possible to achieve the highest possible sintered density ρ for demanding applications. Because of this, high static and cyclic strength values are expected; moreover, the high dimensional accuracy, low surface roughness and high degree of geometrical freedom are key reasons for the widespread use of MIM steel grades for highly-loaded components in the automotive, firearms and medical device industries.

For such parts, with quantities that range from 20,000 to over one million parts a year, it is essential to estimate the fatigue strength at the knee point σ_A. Because MIM components are less porous than conventional 'press and sintered' PM components, material behaviour is influenced more by single defects than by the whole pore size distribution. For this reason, it is important to understand the influence of critical MIM defects on the fatigue strength at the knee point σ_A. It is known that internal defects have a higher effect on the cyclic properties than on the static properties because the material plasticity is suppressed. High-Cycle Fatigue (HCF) experiments are recommended to identify the effects of defects such as non-metallic inclusions from feedstock impurities,

Fig. 1 A view of the continuous debinding and sintering facilities at GKN Sinter Metals' MIM operation in Bad Langensalza, one of the largest in Europe

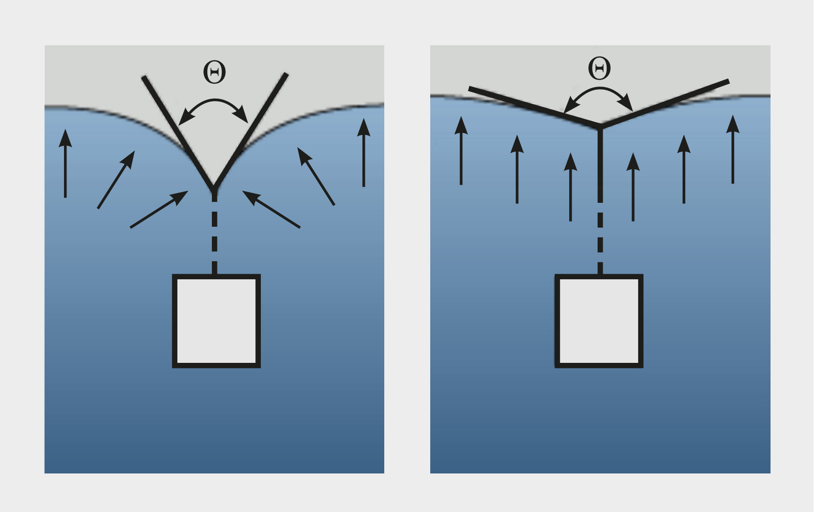

Fig. 2 Internal weld line above an injection moulding tool inlet and characteristic superficial sink mark angle Θ of two welded fill fronts (Image from [2])

shrinkage cavities and weld lines. This is due to the suppressed plastic strain component ε_p during the stress-controlled HCF experiments.

The combination of a purely elastic loading and a high number of cyclic repetitions N will bring all issues of concern to light. However, reliable information on material properties, especially cyclic material properties, is rare for MIM steel grades. The European Powder Metallurgy Association (EPMA) stated in its current 'Introduction to Metal Injection Moulding' promotional brochure: "The European MIM industry is undertaking great efforts to provide design engineers with comprehensive material property data as required by finite element analysis (FEA) and other design software. The determination of these characteristics, in particular fatigue properties, is costly and time consuming. Only limited data are available, for instance for the precipitation hardening stainless steel MIM-17-4PH and the low alloy steel MIM-4340, which is generally heat treated by a conventional quench-and-temper process" [1]. Therefore, an internal programme was initiated in 2016 at GKN Sinter Metals to investigate the static and cyclic material properties of a few common MIM steel grades.

> " The combination of a purely elastic loading and a high number of cyclic repetitions N will bring all issues of concern to light. However, reliable information on material properties, especially cyclic material properties, are rare for MIM steel grades"

MIM 8620 (20NiCrMo2-2) and MIM 100Cr6 are two common MIM steel grades which have found wide application, including for the production of automotive upvalve rockers for Variable Valve Timing (VVT) systems. Because of their geometric complexity, MIM components typically feature many notches, along with inevitable weld lines because of a combination of the injection moulding step and part complexity. A material's property response to these notches and weld lines is of critical importance for the MIM industry.

Moreover, it should be mentioned at this point that fully-reversed (loading ratio R=-1, often realised via rotating bending) fatigue strength at the knee point σ_A values are insufficient for a fatigue assessment and a precise fatigue lifetime calculation. This is due to the fact that most MIM components are loaded with static pre-loads (interference fits, bolts or screws) and superimposed cyclic operating loads. Consequently, higher loading ratios than R=-1, which are more damaging at a similar stress amplitude σ_a, must be tested. This study therefore focuses on three specific areas:

- Providing full fatigue data sets for FEA fatigue lifetime calculations (both HCF and Long Life Fatigue (LLF)), including static properties, mean stress and notch sensitivities and scatter
- Comparison between different strongly notched fatigue specimens
- Investigation of the interface strength of weld lines

Tool design related weld lines

Weld lines are the result of the meeting of two or more fill fronts where the feedstock flow splits and joins together during the filling process [2]. Such weld lines can occur behind drillings (injection moulding tool inlets) or if the component is injection moulded with more than one gate. A good overview regarding the avoidance and the improvement of weld lines can be found in [3]. A few literature sources discuss weld lines as a MIM defect that can influence mechanical properties [4, 5, 6, 7].

R M German differentiates between moulding defects (part sticking, short shots, air pockets and voids, sink marks and internal cracks) and debinding defects (large pores, warpage, distortion, cracks, porosity, rounded edges, carbon issues, surface finish of melted component). Moreover, he concludes that sintering amplifies defects which were introduced earlier in mixing, moulding or debinding [8]. This defect compilation is an extract from a larger overview of defect sources and cures from [9].

The plastic injection moulding industry has a lot of experience with weld lines. They differentiate weld lines formed due to different feedstock flow temperatures ϑ during the fill front formation and weld lines formed by differently angle-orientated fill fronts. If two fill fronts meet each other with a certain angle Θ, a blurred weld line could arise [2]. The resulting part surface shows a local sink mark, which can be interpreted as a notch. In the plastic injection moulding industry, a characteristic sink mark angle of $\Theta=135°$ is used to differentiate between a merged ($\Theta > 135°$) and conventional ($\Theta < 135°$) weld line. Fig. 2 shows a schematic of the corresponding weld line formation. Well-welded fill fronts are assumed to be non-critical [2].

Besides the local sink mark formation, another feature is assumed to be critical: a sharp angle between the meeting fill fronts will also reduce component quality [3]. The damaging effect of weld lines could be dramatic in the plastic injection moulding industry if an anisotropic orientation of a reinforced filling material, such as glass or carbon fibre, is provoked.

In the past, designers of MIM tools moved the gates to positions that ensured weld lines were as far away as possible from highly-loaded regions of a component. Fig. 3, however, shows that this is not always possible. In this case, the weld line is located on a hub which is loaded with a fracture opening mode 1 during the interference fitting. Another option is to vary the gate diameter d or the volumetric injection feedstock flow rate Q to guarantee a quick injection moulding process without a rapid cooling of the feedstock.

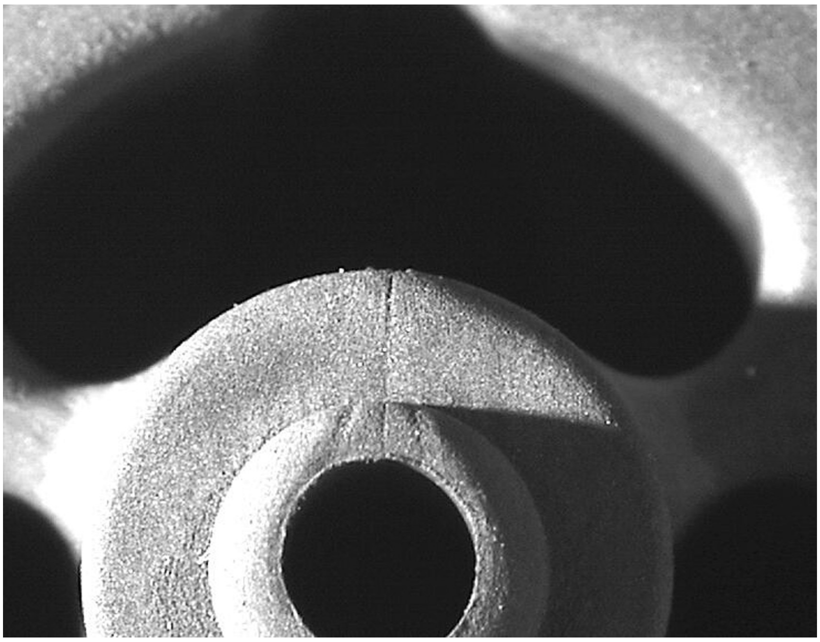

Fig. 3 Weld line and superficial sink mark on a hub of an injection moulded MIM component. Circumferential tensile stresses will load the weld line with fracture opening mode 1 during the interference fitting

Furthermore, the feedstock flow temperature ϑ or the tool temperature ϑ_{tool} can be increased to decrease the feedstock viscosity η. In general, smaller components with shorter feedstock flow paths are favoured since the resulting temperature gradient $\Delta\vartheta$ from the injection gate to the formed weld line is lower. To analyse the injection moulding process in general, and to investigate the resulting feedstock flow paths, a mould flow simulation is an often-recommended procedure [4, 5].

> *"In the past, designers of MIM tools moved the gates to positions that ensured weld lines were as far away as possible from highly-loaded regions of a component..."*

Fig. 4 (a-e) shows the filling evolution and the final weld line position of a twin-gated notched fatigue specimen according to DIN EN ISO 3928 (notch radius r=0.45 mm, stress concentration factor $K_t=3.42$, axial loading mode) simulated with Sigmasoft Mould Flow. With this procedure, the resulting weld line position can be simulated. As a result, the tool designer can vary the gate position. However, the shifting of the weld line to non-critical component regions is not always possible, because of the complexity of the injection moulding tool; in particular, the location of cooling channels, other cavities and the length of the runner. It is, therefore, necessary to assume the worst-

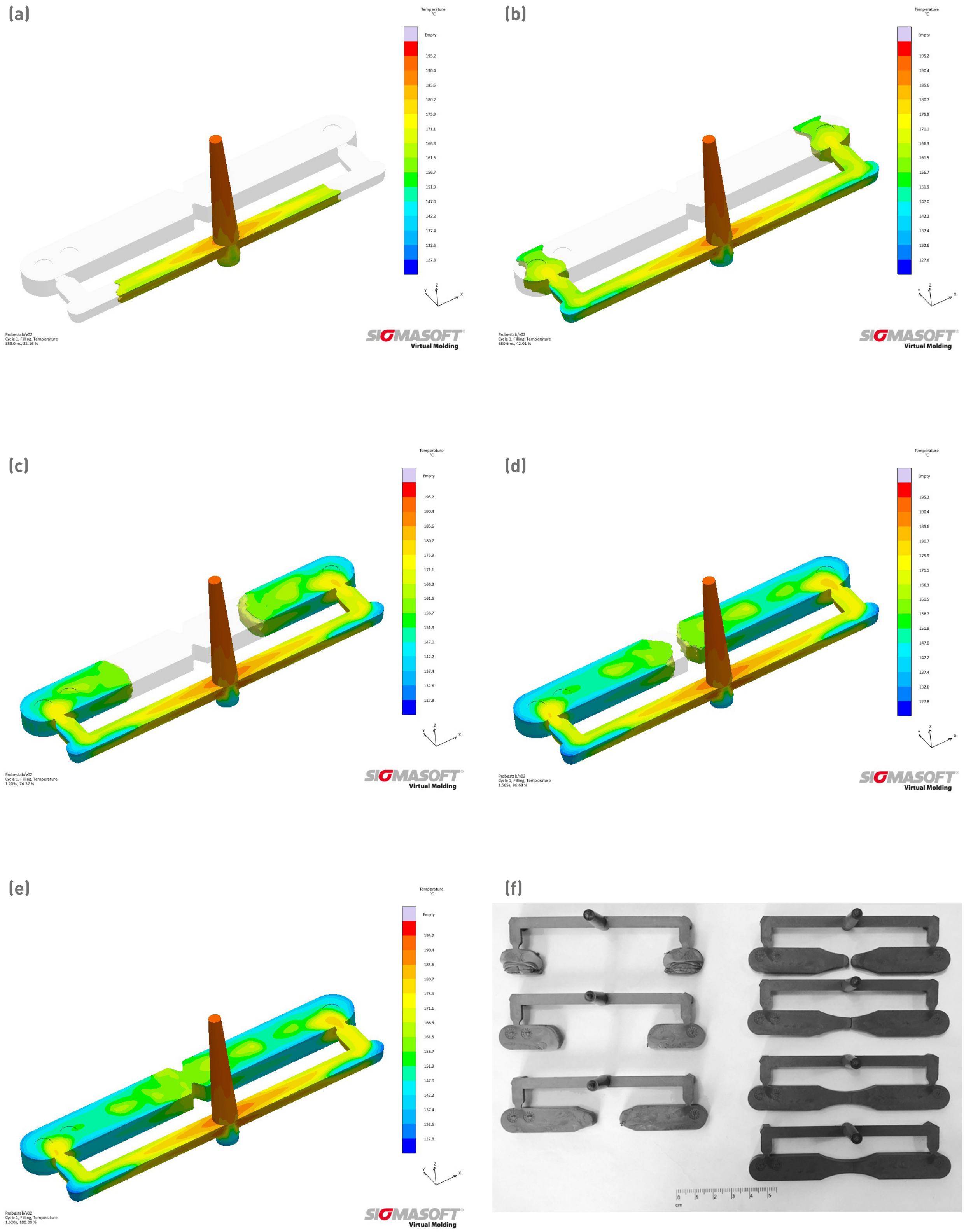

Fig. 4 Filling evolution and final weld line position of a twin-gated notched fatigue specimen according to DIN EN ISO 3928 (notch radius r=0.45 mm, stress concentration factor K_t=3.42, axial loading mode). In this case, the gate diameters were slightly varied to investigate the symmetry of the resulting feedstock flow paths (a-e). f shows an injection moulding study of an unnotched fatigue specimen according to DIN EN ISO 3928 (notch radius r=30 mm, stress concentration factor K_t=1.06, axial loading mode)

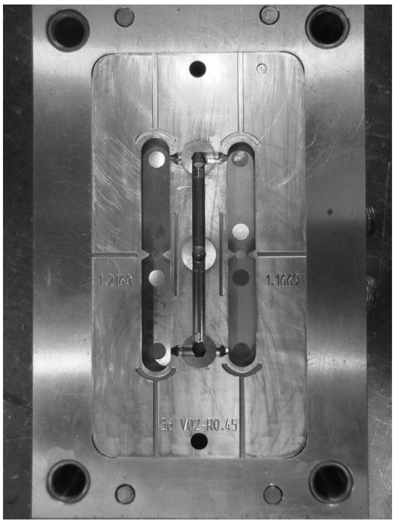

Fig. 5 Tool cavity for the fatigue specimens according to DIN EN ISO 3928 with a notch radius of r=0.45 mm for two different offset factors OF and special adjustable valves

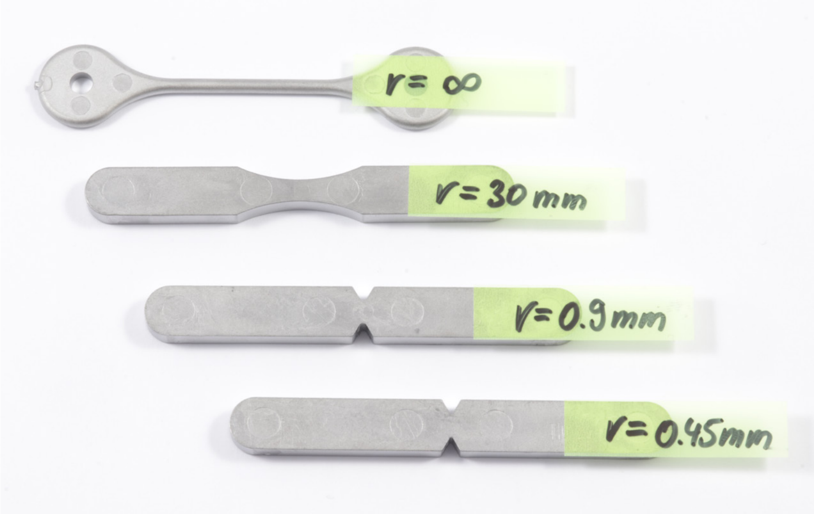

Fig. 6 Overview of the tensile test and fatigue specimens used (from top to bottom): tensile test specimen according to DIN EN ISO 2740 (notch radius r=∞, stress concentration factor $K_t \approx 1$, axial loading mode), unnotched fatigue specimen according to DIN EN ISO 3928 (notch radius r=30 mm, stress concentration factor K_t=1.06, axial loading mode), notched fatigue specimen according to DIN EN ISO 3928 (notch radius r=0.9 mm, stress concentration factor K_t=2.53, axial loading mode) and notched fatigue specimen according to DIN EN ISO 3928 (notch radius r=0.45 mm, stress concentration factor K_t=3.42, axial loading mode). Note that the stress concentration factor K_t depends on the applied load. The defined stress concentration K_t factors above are valid for the axial loading mode (tensile loading mode, Table 1). They are not to be confused with the stress concentration factors from the bending loading mode (Table 2 and Table 3)

case scenario where the weld line is located in the highly-loaded component region and the weld line is loaded with fracture opening mode 1.

High cycle fatigue experiments are rare in the MIM industry. To determine material properties and to investigate the effect of weld lines, a new tool design for fatigue specimens was developed. As a result, there is no standardised fatigue specimen geometry for MIM steel grades available or recommended. Most of the existing fatigue experiments were conducted on turned and ground MIM preforms (cylindrical bars) without consideration of the weld line position. The machining operations are the dominant cost drivers which make fatigue testing expensive. Moreover, the effects from machining, such as providing a smoothing effect, densification, work hardening and the introduction of residual stresses, are not discussed. These effects must be considered, however, since most MIM components are used with as-sintered surfaces.

Therefore, in addition to DIN EN ISO 2740 tensile test specimens, DIN EN ISO 3928 fatigue specimens were also injection moulded with two different gate variants. For the investigation of notch sensitivity and to derive the resulting support factor n_χ, three different tools with different cavities were designed. The unnotched DIN EN ISO 3928 fatigue specimen has a waist with a notch radius of r=30 mm (K_t=1.04 for bending loading). Moreover, two further fatigue specimens with a respective notch radius of r=0.9 mm (K_t=1.91 for bending loading) and r=0.45 mm (K_t=2.47 for bending loading, slightly varying from DIN EN ISO 3928) were produced. The corresponding stress concentration factors K_t were calculated numerically via Finite Element Analysis (FEA). The worst-case scenario discussed above was achieved with the tool cavity shown in Fig. 5. With this injection moulding cavity, it is possible to produce single-gated and twin-gated fatigue specimens by adjusting the valves.

Because of the symmetry of the runners, the resulting weld line of the twin-gated injection moulding process is located at the notch root, as can be seen in Fig. 4. The tool cavity dimensions were corrected with an offset factor OF=1.2160 for MIM 8620 (Catamold 8620 from BASF, 20NiCrMo2-2) and OF=1.1669 for MIM 100Cr6 (Catamold 100Cr6 from BASF) to match the required dimensions of DIN EN ISO 3928.

Specimen production

The two low-alloyed MIM steel grades selected (MIM 8620 case-hardened vs MIM 100Cr6 hardened) were compared, with a focus on the static and cyclic material properties, respectively. The injection moulding of all specimens was undertaken with plant-specific injection moulding parameters. Fig. 6 shows the four manufactured geometries in the as-sintered condition. A more detailed overview of the formed weld lines

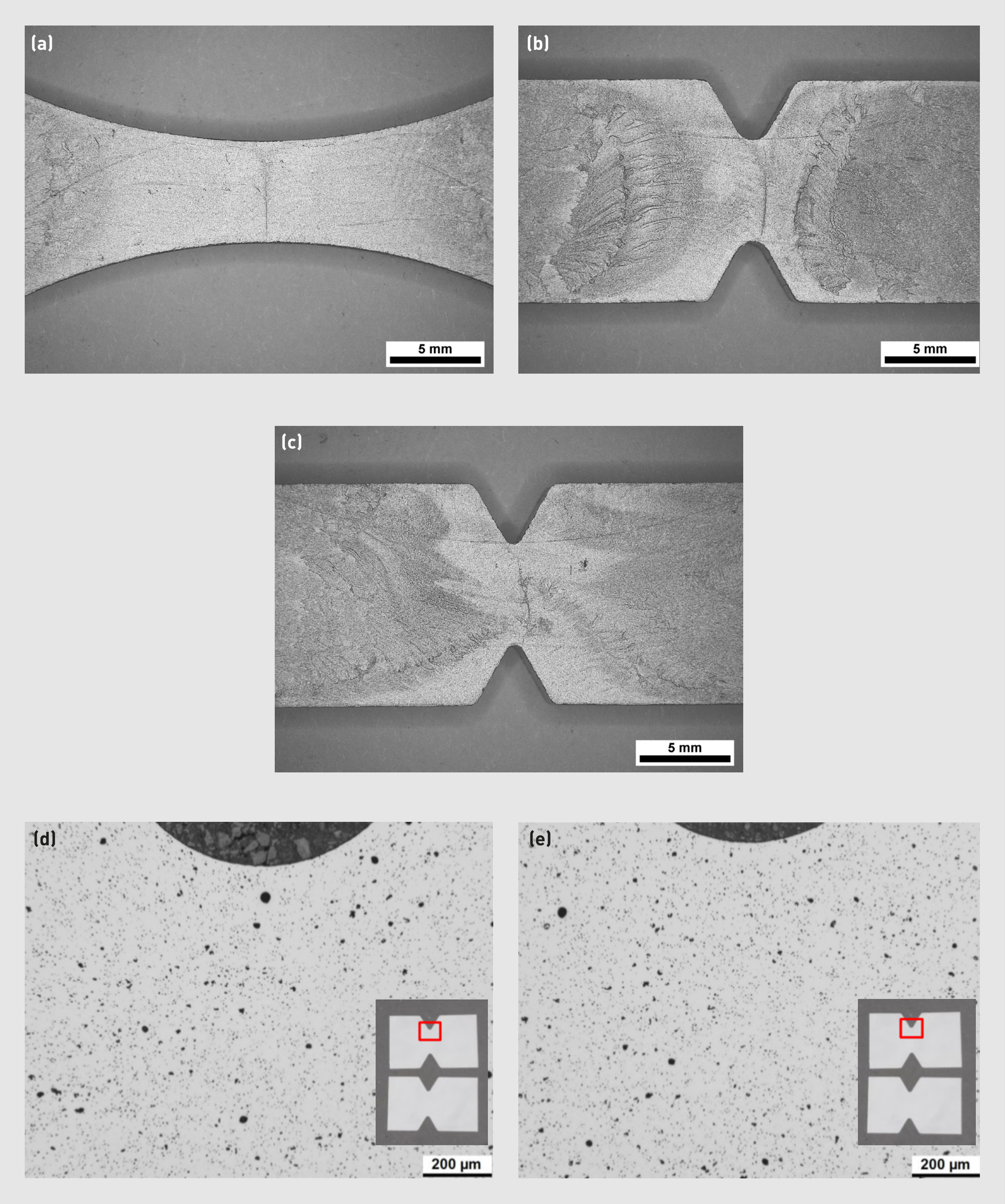

Fig. 7 Visible weld lines and superficial sink marks of twin-gated fatigue specimens according to DIN EN ISO 3928 (from top to bottom) of MIM 8620 as-sintered specimens: unnotched fatigue specimen according to DIN EN ISO 3928 (notch radius r=30 mm, stress concentration factor K_t=1.06, axial loading mode), notched fatigue specimen according to DIN EN ISO 3928 (notch radius r=0.9 mm, stress concentration factor K_t=2.53, axial loading mode) and notched fatigue specimen according to DIN EN ISO 3928 (notch radius r=0.45 mm, stress concentration factor K_t=3.42, axial loading mode) (a-c). Unetched microstructures of MIM 100Cr6 hardened taken in the notch root of a notched fatigue specimen according to DIN EN ISO 3928 (notch radius r=0.45 mm, stress concentration factor K_t=3.42, axial loading mode). d is from a single-gated specimen (maximum Feret diameter $d_{max.\ Feret}$=33 µm) and e is from a twin-gated specimen (maximum Feret diameter $d_{max.\ Feret}$=24 µm). A difference regarding the porosity f, its shape or distribution cannot be observed. This indicates that a recognition of weld lines is more likely from the optical visible impress (colouring) than from the microstructure

is shown in Fig. 7. The single-gated and twin-gated fatigue specimens were injection moulded with the same filling and packing parameters (volumetric injection feedstock flow rate Q, filling pressure p_f, packing pressure profile p_p, filling time t_f and packing time t_p) to ensure similar material properties.

After injection moulding, the densities of the right-hand and left-hand gripping ends were measured by the Archimedes method to guarantee comparable green part densities ρ_g. All specimens were then peened with a plastic granulate to remove the injection moulding burrs. Potential residual stresses σ_R were eliminated by the subsequent sintering process above the recrystallisation temperature of both the MIM steel grades.

Both MIM steel grades were sintered together to achieve the targeted sintered density of ρ=7.4 g/cm^3. Debinding and sintering were performed in a continuous debinding and sintering walking beam furnace. The catalytic debinding of the specimens was carried out in a low temperature atmosphere of HNO_3 and N_2 for t=390 min. The parts were sintered at a sintering temperature of ϑ=1251°C for a sintering time of approximately t=90 min in a 100% N_2 atmosphere with an atmospheric pressure of p=10 mbar. The cooling-rate $\Delta\vartheta/\Delta t_{800\,°C\text{-}600°C}$ was not recorded. After sintering, the specimens made of MIM 8620 were carburised, case-hardened and tempered at an external company.

The carburising atmosphere consisted of natural gas, CH_4O (methanol) and N_2 with a carbon level of C=1%. The carburising temperature ϑ and the carburising time t were not communicated; however, a value of $\vartheta\approx$950°C, the recommended value from the feedstock supplier, BASF SE [10], can be assumed. The quenching medium was oil. Afterwards, the specimens were tempered at ϑ=170°C for t=2 h.

The sintered MIM 100Cr6 specimens were processed using a different route. They were austenitised, quenched and tempered by an external company. The austenitisation temperature ϑ and the austenitisation time t were not communicated. The quenching medium was oil. Further details regarding the tempering were not communicated. The nitrogen, oxygen and carbon contents were measured after sintering and after the heat treatments.

The complete carbon profile C(d) of MIM 8620 case-hardened was not measured. The surface carbon content C_0 of MIM 8620 case-hardened cannot be measured precisely with the Leco carbon combustion technique. Therefore, a local equilibrium was assumed with $C_0\approx$C-level=1%. The core carbon content was measured as $C_\infty\approx$0.146%. Therefore, a sigmoidal carbon profile C(d) with an asymptotic plateau in the core region can be assumed.

MIM 100Cr6 hardened exhibits a value of $C_0\approx C_\infty\approx$0.85%. Moreover, both MIM steel grades show a small nitrogen pick-up of approximately $N_0\approx N_\infty\approx$0.03%. This could be explained by the chemical compositions of both the MIM steel grades and the affinity of chromium for nitrogen. MIM 8620 contains Cr=0.5% and MIM 100Cr6 contains Cr=1.5%, respectively.

Static properties and resulting notch-strength ratios γ

Material toughness is an important property because it characterises a material's resistance to crack growth and rupture as well as its ability to absorb energy in the form of plastic deformation. This is a very general definition. However, several metrics are used to characterise material toughness, for example:

- Plastic strain ε_p from the stress-strain curve
- The equivalent strain energy density ESED from the stress-strain curve (integral of the stress-strain curve)
- The fracture toughness K_{Ic} and the cyclic stress intensity threshold ΔK_{th} from static and cyclic fracture mechanics tests
- The impact strength W or toughness W/A from Charpy or Izod impact strength tests and special drop-weight tests to imitate the behaviour of welded sheets (Pellini and Battelle drop-weight tests)

Unfortunately, the correlation between all these toughness metrics is not very good. This leads to the conclusion that there is no single 'material toughness'. Therefore, the testing method should be as close as possible to the real application and the real loading, with special consideration of the environment (humidity, temperature and pH value), the strain rate $\Delta\varepsilon/\Delta t$ (impact), the geometry (notches) and the existence of defects (cracks, flaws or welding seams).

MIM components are filigree and very complex in shape. From the mechanical point of view, they are notched in multiple ways. As a consequence, a toughness metric is needed to characterise its response on multiaxial stress states and on the local peak stresses $\sigma=K_t*\sigma_n$ ('stress raisers') with sharp stress gradients $\chi*\sim 1/r$. An additional and very easy testing method is based on a comparison between the ultimate tensile strength σ_u of unnotched tensile test specimens ($\sigma_{u,\,smooth}$, $K_t\approx1$, axial loading mode, smooth condition) and notched fatigue specimens ($\sigma_{u,\,notched}$, $K_t>1$, axial loading mode, notched condition). The ratio is called the notch-strength ratio γ and depends on the material, the heat-treatment condition and on the notch geometry (flat or circumferential notch and sharpness of the notch/notch radius r) and is defined as [11]:

$$\gamma = \frac{\sigma_{u,notched}}{\sigma_{u,smooth}}$$

For perfectly brittle materials, the notch-strength ratio γ follows the perfectly brittle limit hyperbola as a function of the realised stress concentration factor K_t:

$$\gamma_{brittle} = \frac{1}{K_t} = \frac{\sigma_{u,notched}}{\sigma_{u,smooth}}$$

Material	Geometry	r (mm), K_t (1), axial	Condition	σ_u (MPa), 1 gate	σ_u (MPa), 2 gates
MIM 8620	DIN EN ISO 2740	∞, $K_t\approx1$	As-sintered	397	Not realised
MIM 8620	DIN EN ISO 3928	30, $K_t=1.06$	As-sintered	418	417
MIM 8620	DIN EN ISO 3928	0.9, $K_t=2.53$	As-sintered	458	447
MIM 8620	DIN EN ISO 3928	0.45, $K_t=3.42$	As-sintered	432	441
MIM 8620	DIN EN ISO 2740	∞, $K_t\approx1$	Case-hardened	1102	Not realised
MIM 8620	DIN EN ISO 3928	30, $K_t=1.06$	Case-hardened	915	947
MIM 8620	DIN EN ISO 3928	0.9, $K_t=2.53$	Case-hardened	802	781
MIM 8620	DIN EN ISO 3928	0.45, $K_t=3.42$	Case-hardened	703	725
MIM 100Cr6	DIN EN ISO 2740	∞, $K_t\approx1$	As-sintered	1076	Not realised
MIM 100Cr6	DIN EN ISO 3928	30, $K_t=1.06$	As-sintered	1035	1063
MIM 100Cr6	DIN EN ISO 3928	0.9, $K_t=2.53$	As-sintered	1045	1048
MIM 100Cr6	DIN EN ISO 3928	0.45, $K_t=3.42$	As-sintered	923	939
MIM 100Cr6	DIN EN ISO 2740	∞, $K_t\approx1$	Hardened	1106	Not realised
MIM 100Cr6	DIN EN ISO 3928	30, $K_t=1.06$	Hardened	1033	1022
MIM 100Cr6	DIN EN ISO 3928	0.9, $K_t=2.53$	Hardened	629	610
MIM 100Cr6	DIN EN ISO 3928	0.45, $K_t=3.42$	Hardened	470	432

Table 1 Static tensile test results as a function of the material (MIM steel grades), material condition (heat treatment condition), notch radius r and the weld line position (1 gate vs 2 gates)

The notch-strength ratio γ correlates with the plastic strain ε_p and the macro-hardness H of the material. Harder materials exhibit a lower ductility. They show a stronger drop of the notch-strength ratio γ [11]. This means that those materials are more sensitive to peak stresses $\sigma=K_t*\sigma_n$ ('stress raisers') and a shape optimisation of the MIM component (e.g. Baud curve, Mattheck's tensile triangles or other splines) is highly recommended to reduce the peak stresses $\sigma=K_t*\sigma_n$. However, for most material and notch geometry combinations, the notch-strength ratio is $\gamma<1$. This indicates the assumed notch weakening effect. In the case of very soft and ductile materials, the plastic constraint effect can be recognised. In this case, the notch-strength ratio is $\gamma>1$ and a notch strengthening can be observed.

The static material properties were characterised in terms of the stress-strain and the stress-displacement response. As a reference, single-gated tensile test specimens according to DIN EN ISO 2740 were tested in the as-sintered and the case-hardened (MIM 8620 case-hardened) or hardened (MIM 100Cr6 hardened) conditions. These static tensile tests were conducted according to the existing standards and correct stress-strain curves could be derived.

Additionally, non-conforming static tensile tests on notched (waist with a notch radius of r=30 mm, r=0.9 mm and r=0.45 mm) fatigue specimens according to DIN EN ISO 3928 were conducted to investigate the interface strength and the notch sensitivity (in terms of the notch-strength ratio γ). Moreover, the difference between the single-gated and the twin-gated specimens can be allocated to the weld line position.

The two MIM steel grades exhibited almost the same surface macro-hardness H after the heat-treatment. The surface macro-hardness was found to be H=631 HV 30 for MIM 8620 case-hardened and H=626 HV 30 for MIM 100Cr6 hardened, respectively (averaged values between all realised geometries given in Table 1). This indicates a comparable apparent surface carbon content C_0 after the heat-treatment and comparable quenching conditions, because the maximum achievable surface hardness H_{max} is just a function of the surface carbon content C_0 and shows no strong effect from the alloying element content.

This finding agrees well with the applied carbon level of C-level=1% of the carburising atmosphere (MIM 8620 case-hardened) and the alloyed carbon content of C=1% (MIM 100Cr6 hardened). Even if MIM 8620 case-hardened must be assumed as a multilayer material (in contrast to the homogeneous MIM 100Cr6 hardened material variant) with location-dependent material properties due to the continuous carbon profile C(d), it is interesting to note that the ultimate tensile strength σ_u values are almost identical.

However, case-hardened (in general surface treated) materials should be characterised by their micro-hardness profile H(d) because of their

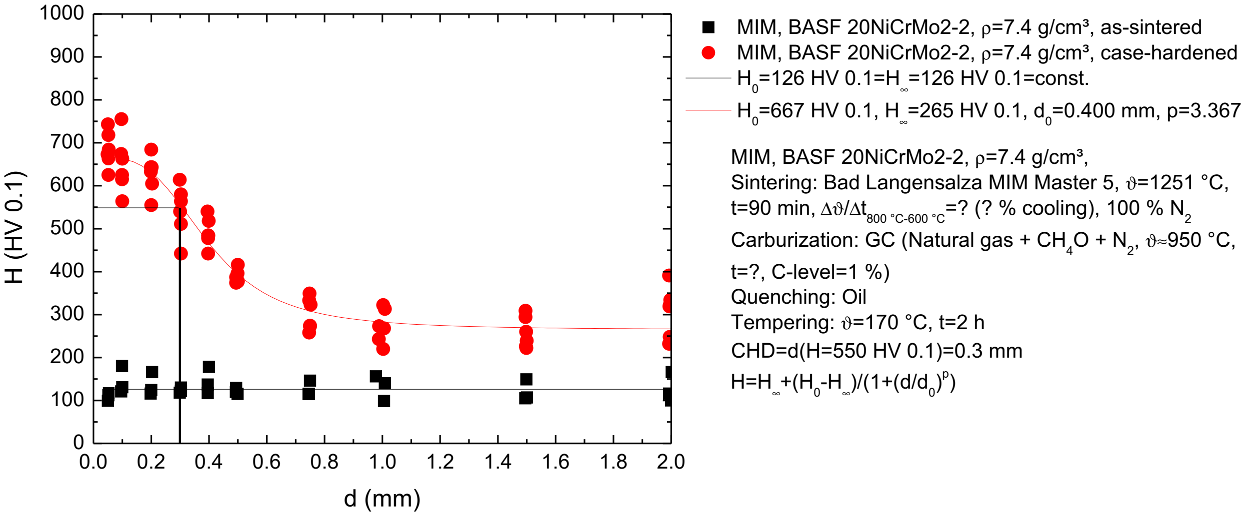

Fig. 8 Micro-hardness profiles H(d) of MIM 8620 (here denoted as 20NiCrMo2-2) with a sintered density of ρ=7.4 g/cm³ before (as-sintered condition) and after the case-hardening (case-hardened condition). The carburising time t was not communicated (marked with a question mark)

gradient material properties. Fig. 8 shows the micro-hardness profiles H(d) of MIM 8620 case-hardened with a sintered density of ρ=7.4 g/cm³ before (as-sintered condition) and after the case-hardening (case-hardened condition). The micro-hardness profile H(d) according to DIN EN ISO 4507 was approximated with a sigmoidal power-law as:

$$H(d) = H_\infty + \frac{(H_0 - H_\infty)}{\left(1 + \left(\frac{d}{d_0}\right)^p\right)}$$

In this equation, the first asymptote H_∞ denotes the core micro-hardness, the second asymptote H_0 denotes the surface micro-hardness, d_0 is the inflection point of the sigmoidal function and p is the slope. The derived parameters are given in Fig. 8. It can be seen that a surface micro-hardness of H_0=667 HV 0.1, a core micro-hardness of H_∞=265 HV 0.1 and a case-hardening depth of CHD_{550}=d(H=550 HV 0.1)=0.3 mm were achieved after the case-hardening. In the as-sintered condition, the sigmoidal shaped curve decreases to a line with identical surface micro-hardness H_0 and core micro-hardness H_∞ values with H_0=H_∞=126 HV 0.1=const.

Due to its homogeneous alloyed carbon content of C=1%, MIM 100Cr6 hardened was actually through-hardened. This results in identical surface micro-hardness H_0 and core micro-hardness H_∞ values with H_0=H_∞=705 HV 0.1=const. However, even in the macro-hardness domain, both MIM steel grades exhibit similar surface macro-hardness H values (H=631 HV 30 for MIM 8620 case-hardened vs H=626 HV 30 for MIM 100Cr6 hardened). The effect from the load (HV 30 vs HV 0.1) can be allocated to the sintered density of ρ=7.4 g/cm³ (porosity f). The macro-hardness H is an apparent hardness value in the sense of a combination of the metallic matrix hardness and the porosity hardness. Therefore, those macro-hardness H values (HV 30) are lower.

The ultimate tensile strength σ_u of MIM 100Cr6 hardened is σ_u=1106 MPa and the ultimate tensile strength σ_u of MIM 8620 case-hardened is σ_u=1102 MPa (Table 1), respectively (tensile test specimen according to DIN EN ISO 2740, 1 gate). This could indicate a through-hardening effect for the MIM 8620 case-hardened material variant due to the small cross-section of the DIN EN ISO 2740 specimen. However, the corresponding case-hardening depth was found to be CHD_{550}=0.3 mm, whereas the DIN EN ISO 2740 specimen diameter is d≈3 mm (d=3.8 mm in the green state). This means that the generated micro-hardness profile H(d) is close to the through-hardening condition 2*CHD_{550}=d. In comparison to the achieved high surface macro-hardness H values after the heat-treatments, the derived ultimate tensile strength σ_u values seem to be too low. According to the often-proposed σ_u≈3*H correlation, ultimate tensile strength σ_u values of approximately σ_u≈1800 MPa were expected.

It is interesting to note that the ultimate tensile strength σ_u of MIM 100Cr6 remains the same in the as-sintered and the hardened material condition, respectively (σ_u=1076 MPa for the as-sintered condition vs σ_u=1106 MPa for the hardened condition, tensile test specimens according to DIN EN ISO 2740, 1 gate). Nevertheless, the ductility (in terms of the fracture strain ε_f) has changed dramatically (ε_f=7.43% for the as-sintered condition vs ε_f=0.88% for the hardened condition, tensile test specimens according to DIN EN ISO 2740, 1 gate). This is remarkable because the often-proposed σ_u≈3*H correlation fails [12]. The surface macro-hardness of MIM 100Cr6 could be increased from H=273 HV 30 in the as-sintered condition to H=626 HV 30 in the hardened condition.

In this context, it is worth considering a potential correlation between the unnotched fully reversed bending fatigue strength at the knee point σ_A

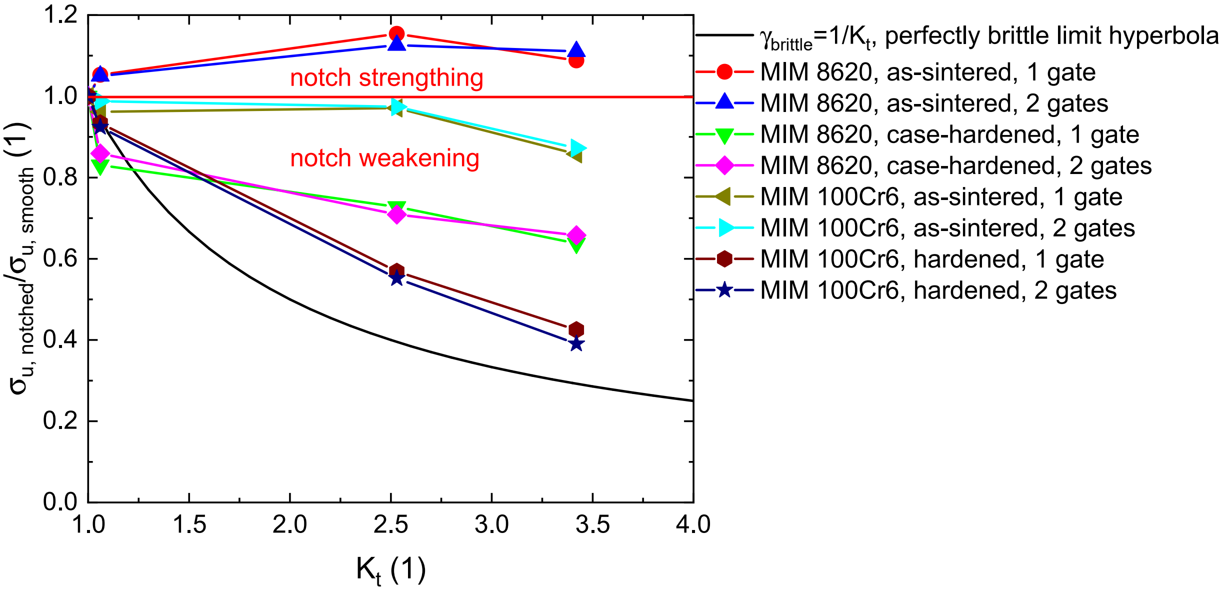

Fig. 9 Notch-strength ratios γ of the tested MIM steel grades. MIM 8620 as-sintered exhibits a notch strengthening effect due to its low macro-hardness H and low-alloyed carbon content of C=0.2% in the as-sintered material condition. MIM 100Cr6 as-sintered shows a neutral behaviour and a slight notch weakening effect at higher stress concentration factors K_t in the as-sintered material condition. Both MIM steel grades show a notch weakening effect after the heat treatments (case-hardening and hardening), whereas MIM 100Cr6 hardened shows a dramatic drop towards the perfectly brittle limit hyperbola. The tensile test specimens according to DIN EN ISO 2740 were only produced without a weld line (single gate). Since a difference regarding the weld line position (single-gate vs twin-gated) tensile test specimens on the static tensile test results cannot be found, the same value was taken as a reference for the unnotched tensile test specimens ($\sigma_{u,\ smooth}$, $K_t \approx 1$, axial loading mode, smooth condition) which were produced with a weld line (twin-gated)

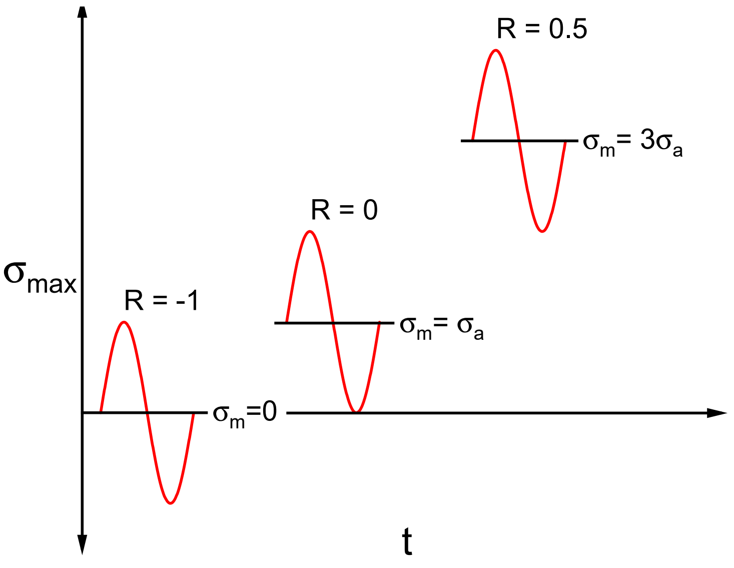

Fig. 10 Loading ratios R during the cyclic bending fatigue experiments. The maximum stress σ_{max} is the sum of the mean stress σ_m (static stress component) and the stress amplitude σ_a (cyclic stress component). The loading ratio R indicates the ratio between the static and the cyclic stress component. Positive loading ratios R indicate positive (tensile) mean stresses σ_m, which are more damaging than negative (compression) mean stresses σ_m with the same stress amplitude σ_a

and a static strength parameter, for example the surface macro-hardness H or the ultimate tensile strength σ_u. If there is a correlation between the unnotched fully reversed bending fatigue strength at the knee point σ_A and the ultimate tensile strength σ_u, similar unnotched fully reversed bending fatigue strengths at the knee point σ_A values would be expected for the two different material conditions (as-sintered vs hardened). This will be not the case. Therefore, it is assumed that a correlation with the surface macro-hardness H will deliver a better agreement. A systematic trend regarding the weld line position (single-gated vs twin-gated tensile test specimens) on the static tensile test results cannot be found. A dramatic difference between the two investigated MIM steel grades occurs in the case of notches or other stress concentrations.

R (1)	K_t (1)	k (1)	N_K (1)	σ_A (MPa)	s_{SAFD} (MPa)	k (1)	N_K (1)	σ_A (MPa)	s_{SAFD} (MPa)
		1 gate				2 gates			
-1	1.04	-19.227	3303592	610.78	7.99	-14.745	3072990	565.55	18.82
0	1.04	-6.213	172096	362.49	15.08	-7.560	309596	333.49	9.58
0.5	1.04	-6.981	198094	195.48	8.72	-4.228	128227	194.46	10.30
-1	1.91	-6.520	146430	468.72	10.59	-5.643	138222	470.39	18.29
-1	2.47	-5.673	124389	423.18	13.02	-5.405	140835	397.07	12.84

Table 2 Basquin parameters for MIM 8620 case-hardened with a sintered density of ρ=7.4 g/cm³ of the derived bending s-N lines (each bending s-N line was derived with n=50 specimens) as function of the weld line position (1 gate vs 2 gates)

R (1)	K_t (1)	k (1)	N_K (1)	σ_A (MPa)	s_{SAFD} (MPa)	k (1)	N_K (1)	σ_A (MPa)	s_{SAFD} (MPa)
		1 gate				2 gates			
-1	1.04	-22.540	521870	624.90	13.13	-0.582	28913	600.85	12.88
0	1.04	-5.901	42219	361.24	9.44	-13.792	102833	382.32	9.63
0.5	1.04	-10.396	88671	215.00	8.34	-6.360	39089	221.04	10.30
-1	1.91	-4.328	41391	412.85	15.55	-4.448	48305	370.68	18.28
-1	2.47	1.398	11503	308.67	9.19	-3.751	67069	301.09	8.54

Table 3 Basquin parameters for MIM 100Cr6 hardened with a sintered density of ρ=7.4 g/cm³ of the derived bending s-N lines (each bending s-N line was derived with n=50 specimens) as function of the weld line position (1 gate vs 2 gates)

The notch-strength ratio γ (for the sharpest produced notch with a notch radius of r=0.45 mm and a corresponding axial stress concentration factor of K_t=3.42 for the axial loading mode, 1 gate) of MIM 100Cr6 hardened reduces to $\gamma=\sigma_u(K_t=3.42)/\sigma_u(K_t\approx1)$=470 MPa/1106 MPa=0.42, whereas MIM 8620 case-hardened exhibits a value of $\gamma=\sigma_u(K_t=3.42)/\sigma_u(K_t\approx1)$=703 MPa/1102 MPa=0.64. In general, the notch-strength ratio γ of MIM 100Cr6 hardened follows the expected progression [11]. From Fig. 9, it can be seen that its behaviour is closer to the perfectly brittle limit hyperbola $\gamma_{brittle}=1/K_t$. This means that the behaviour of MIM 8620 case-hardened differs from expectations. It seems that the higher core ductility and the compressive residual stresses σ_R^- on the surface of MIM 8620 case-hardened effectively decelerate the crack growth in the static loading case. This important effect remains undetected if only standard-conforming static tensile tests are performed. The conclusion for the practical static strength assessment is that MIM 100Cr6 hardened will show a much higher sensitivity to notches or other stress concentrations. This is a clear disadvantage, especially for complex-shaped MIM components.

Cyclic properties

The cyclic material properties were evaluated exactly as described in [13]. Both MIM steel grades were cyclically tested (bending loading mode) with three different loading ratios R (R=-1, R=0 and R=0.5) as shown in Fig. 10.

The notched fatigue specimens according to DIN EN ISO 3928 (K_t=1.91 and K_t=2.47 for the bending loading mode) were only tested with a loading ratio of R=-1 because the Haigh damage lines will be shifted in a more or less parallel manner [14]. Two different batches were produced with a special injection moulding cavity. With this injection moulding cavity (Fig. 5), it is possible to produce single-gated and twin-gated fatigue specimens by adjusting the valves. Further details can be found in [13]. It was the goal to investigate the interface strength of the twin-gated weld lines because weld lines are a common feature of injection moulded MIM components. Moreover, weld lines are assumed to be a MIM defect (critical hot spot) which affects (lowers) the static and cyclic material properties.

The results are summarised in Table 2, with values taken from [13] and Table 3 in terms of the Basquin parameters of the corresponding bending s-N lines where k denotes the slope and N_K the cut-off point. For each bending s-N line, a total number of n=50 specimens (n=25 specimens for the staircase test domain/LLF domain and n=25 for the HCF domain) were used. The bending s-N lines were approximated with the Basquin power-law as:

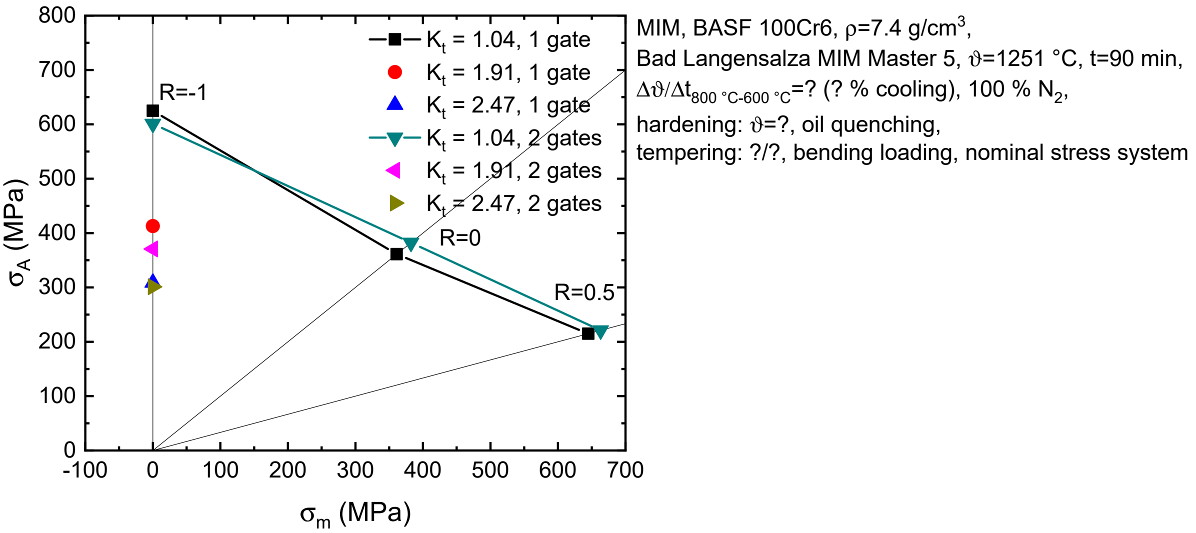

Fig. 11 Haigh damage lines for MIM 100Cr6 hardened (1 gate vs 2 gates) according to the presented values from Table 3 (the cooling-rate $\Delta\vartheta/\Delta t_{800°C\text{-}600°C}$, the austenitisation temperature ϑ, the austenitisation time t and the tempering conditions were not communicated)

$$\sigma_a = \left(\frac{N}{N_K}\right)^{\frac{1}{k}} \sigma_A$$

The bending fatigue strength at the knee point σ_A was derived for a survival probability of P_s=50%. With the help of the standard deviation of the strength s_{SAFD} (note this is only the material scatter without the consideration of the process scatter), the measured bending fatigue strength at the knee point σ_A=σ_A(P_s=50%) and a tabulated parameter (Gaussian quantile u), a conversion into all other required survival probability levels P_s is possible:

$$\sigma_A(P_s) = \sigma_A(P_s = 50\%) + u \times s_{SAFD}$$

The unnotched fatigue specimen according to DIN EN ISO 3928 exhibits a waist with a notch radius of r=30 mm (K_t=1.04 for the bending loading mode). Moreover, two further fatigue specimens with a notch radius of r=0.9 mm (K_t=1.91 for the bending loading mode) and r=0.45 mm (K_t=2.47 for the bending loading mode, slightly varying from DIN EN ISO 3928) were produced, respectively.

From the presented values from Table 2 and Table 3 it is evident that both MIM steel grades exhibit a similar material scatter. This material scatter is defined in terms of the standard deviation of the strength s_{SAFD} as described in [15, 16]. The overall variants averaged values, $\overline{s}_{SAFD}$=12.52 MPa for MIM 8620 case-hardened and $\overline{s}_{SAFD}$=11.53 MPa for MIM 100Cr6 hardened, are very similar. This indicates a comparable material and manufacturing quality without larger defects or value variations.

The values are, however, significantly higher than those for conventional 'press and sintered' PM steel grades. As proposed in [15], it seems that there is a rough trend, even if statistically insignificant, that the standard deviation of the strength s_{SAFD} increases with an increasing surface macro-hardness H. A possible explanation for this observation could be the finding that, for most statistical probability density distributions, the mean value μ (here: fatigue strength at the knee point σ_A) and the corresponding standard deviation s (here: the standard deviation of the strength s_{SAFD}) are not completely independent of each other.

A comparison between the two types of gates (single gate vs twin-gates) exhibits only a small effect of the weld lines. Only an averaged drop of the fatigue strength at the knee point σ_A of $\Delta\sigma_A$=-4.3% can be observed for MIM 8620 case-hardened and of $\Delta\sigma_A$=-1.6% for MIM 100Cr6 hardened, respectively, whereas this effect is not systematic. This means that not all twin-gated bending fatigue strengths at the knee point σ_A values exhibit a drop of the cyclic material properties. This observation is based on small injection moulded fatigue specimens and means that the effect of weld lines can be neglected for smaller MIM components if the difference between the feedstock flow temperatures ϑ is small and a sufficient welding can be assumed.

The remaining Basquin parameters of the corresponding bending s-N lines should be discussed very briefly. The slope k and the cut-off point N_K are essential for damage accumulation calculations if a load spectrum with varying stress amplitudes σ_a is considered. MIM 8620 case-hardened exhibits very flat bending s-N lines for the unnotched (K_t=1.04 for the bending loading mode) fully reserved loading case (R=-1). This holds true for both weld line positions (1 gate vs 2 gates). As a result, the slopes k are very small (1 gate: k=-19.227 and 2 gates: k=-14.745) and the cut-

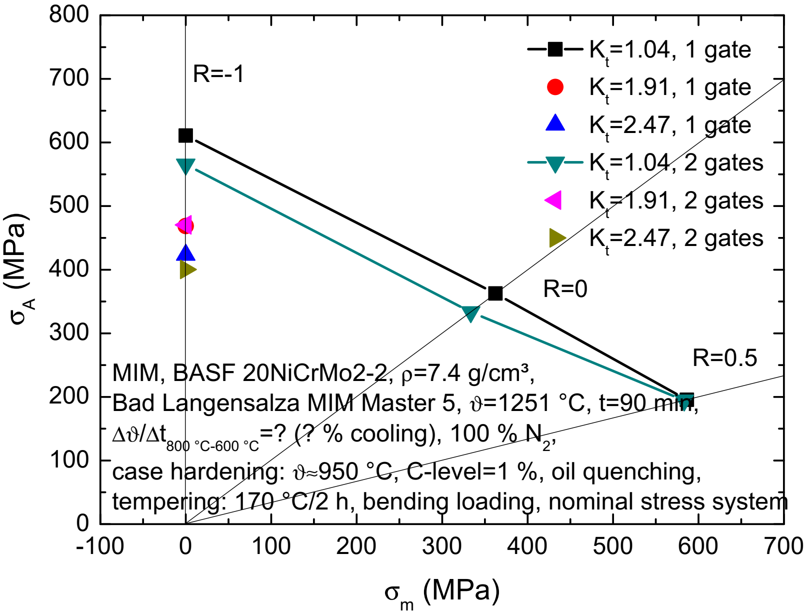

Fig. 12 Haigh damage lines for MIM 8620 (here denoted as 20NiCrMo2-2) case-hardened (1 gate vs 2 gates) according to the presented values from Table 2 (the cooling-rate $\Delta\vartheta/\Delta t_{800°C-600°C}$, the austenitisation temperature ϑ, the austenitisation time t and the tempering conditions were not communicated)

off points N_K are shifted to very high numbers (1 gate: N_K=3303592 and 2 gates: N_K=3072990). A variation, in terms of the loading ratio R or in terms of the stress concentration factor K_t, change the observed tendencies completely. The resulting bending s-N lines are much steeper with much higher slopes k and smaller cut-off points N_K.

The other slopes k vary between k=-4.228 and k=-7.560. However, MIM 8620 case-hardened behaves in a tolerant manner, because all cut-off points are larger than N_K=124389. Therefore, damage accumulation calculations seem to be possible. MIM 100Cr6 hardened behaves more unpredictably. In general, the cut-off points N_K are much smaller than those from MIM 8620 case-hardened. As a result, damage accumulation calculations must be avoided. Moreover, two slopes k (1 gate/R=-1/K_t=2.47: k=1.398 and 2 gates/R=-1/K_t=1.04: k=-0.582) are wrong. Even if n=25 specimens were available for the HCF domain, the SAFD software algorithm [15] was not able to approximate a best fit line for the data points.

This means that, for MIM 100Cr6 hardened, there is only a small transition zone between the HCF domain and the LLF domain. Therefore, MIM components made of MIM 100Cr6 hardened should be designed for LLF loadings only. From the data values presented in Table 2 and Table 3, the corresponding Haigh damage lines can be constructed, and the corresponding mean stress sensitivities M can be calculated according to the FKM guideline [17].

For MIM 8620 case-hardened, the mean stress sensitivities M can be quantified as M_2=0.69 (1 gate) and M_2=0.70 (2 gates) and M_3=0.75 (1 gate) and M_3=0.56 (2 gates), respectively. MIM 100Cr6 hardened exhibits similar values with M_2=0.73 (1 gate) and M_2=0.57 (2 gates) and M_3=0.52 (1 gate) and M_3=0.57 (2 gates), respectively. Fig. 11 exhibits the Haigh diagram for MIM 100Cr6 hardened. This Haigh diagram can be compared with its MIM 8620 case-hardened counterpart from Fig. 12. If the averaged (between the two gate variants) values are compared, it is found that MIM 8620 case-hardened behaves with slightly more mean stress sensitivity beyond M_2. However, the unnotched bending fatigue strength at the knee point σ_A values are very similar for the three tested loading ratios R (R=-1, R=0 and R=0.5).

A clear difference between the two tested MIM steel grades arises if the notched bending fatigue strength at the knee point σ_A values are compared. It is evident that MIM 100Cr6 hardened shows a stronger reaction to notches or other stress concentrations. For example, for a stress concentration factor of K_t=2.47, the bending fatigue strength at the knee point σ_A values of MIM 8620 case-hardened are approximately $\Delta\sigma_A\approx100$ MPa higher than those of MIM 100Cr6 hardened. This means that there is a high support effect for MIM 8620 case-hardened.

Contrary to expectations, the MIM 8620 case-hardened material is not perfectly notch sensitive. Due to the high sintered density of ρ=7.4 g/cm³ and the high surface micro-hardness of H_0=667 HV 0.1 a high notch sensitivity was expected. The notch factors are $K_f(K_t=1.91)$=1.30 (1 gate), $K_f(K_t=1.91)$=1.20 (2 gates), $K_f(K_t=2.47)$=1.44 (1 gate) and $K_f(K_t=2.47)$=1.42 (2 gates). Obviously, the notch sensitivity and the resulting support factors n_χ are in the same range as for conventional PM steel grades [14]. It must be investigated whether the material itself (hard surface with soft core) or the resulting compressive residual stresses σ_R^- after the case-hardening are responsible for this observation.

MIM 100Cr6 hardened shows a completely different behaviour. This MIM steel grade was through-hardened to a surface micro-hardness of $H_0=H_\infty$=705 HV 0.1=const. As a result, there is no soft core, which could act as a fatigue crack arrester. Moreover, due to its homogeneous alloyed carbon content of C=1%, the martensitic transformation occurs at the same temperature ϑ. As a result, no beneficial compressive residual stresses σ_R^- will be established on the surface. However, the notch factors K_f are much higher than those from MIM 8620 case-hardened and closer to the linear elastic limit, which is given by the stress concentration factor K_t.

The notch factors are $K_f(K_t=1.91)=1.51$ (1 gate), $K_f(K_t=1.91)=1.62$ (2 gates), $K_f(K_t=2.47)=2.02$ (1 gate) and $K_f(K_t=2.47)=2.00$ (2 gates). The final conclusion regarding the cyclic material properties is very similar to that from the static material properties: MIM 8620 case-hardened shows a much lower notch sensitivity than MIM 100Cr6 hardened. Therefore, this material and material condition is to be favoured. The derived cyclic material properties and model parameters can be used for FEA fatigue lifetime calculations. Only a small modification is needed to transform the bending fatigue strength at the knee point σ_A values into its axial and stress gradient free counterpart. This procedure is described in [14].

Outlook and future work

The values presented above were experimentally derived under the special consideration of the weld line position and the achieved sintered density of $\rho=7.4$ g/cm³. The weld line was assumed as a MIM defect without the definition of its size. Therefore, the location was defined but not the size. This is incomplete information. As a result, an inter- or extrapolation to other defect sizes is not possible. However, a quick prediction or estimation method is needed to approximate the fatigue response in the case of larger defects. The Murakami approach predicts the fully reversed properties (most of the underlaying experiments from Murakami were derived during rotating bending fatigue experiments (R=-1)), therefore, the predicted fully reversed fatigue strength at the knee point σ_A is (for the bending loading mode) bending fatigue strength at the knee point σ_A as a function of the material macro-hardness H (Vickers hardness) and the projected defect area in the first principal direction $(AREA)^{0.5}$.

The position of the defect (surface defect or internal defect) affects a model-inherent factor. Surface cracks, having the same projected defect area $(AREA)^{0.5}$ in the first principal direction, are more critical than comparable internal defects. As a result, the model-inherent factor varies between X=1.43 (surface defect) and X=1.56 (internal defect). Therefore, the predicted bending fatigue strength at the knee point σ_A is lower in the case of a surface defect. The definition of 'defect' is very wide and incorporates cracks, pores, non-metallic inclusions, soft domains in a harder matrix, grain boundary precipitations and surface roughness [18, 19, 20]. An intermediate position is also defined in [18].

Internal defects in contact with the surface should exhibit a factor of X=1.41. It is not clear why this value should be smaller than that from the surface defect (X=1.43). As a result, the factor of X=1.41 is rarely used in practice [19]. However, A. Bergmark assumes X=1.41 for edge defects [20]. The Murakami approach predicts the bending fatigue strength at the knee point σ_A for a fully dense material exhibiting a single defect. The macro-hardness H is a common metric to define the corresponding hardness H of fully dense materials ($H_{macro} \approx H_{micro}$).

However, two modifications are needed to tailor the Murakami approach for sintered and porous PM and MIM steel grades. The effect of the porosity f, which is characteristic for sintered and porous PM and MIM steel grades, has not yet been covered. The first modification is in regard to the required macro-hardness H value. The macro-hardness H is the apparent hardness (superimposition of the porosity and the metallic matrix hardness) in the case of sintered and porous PM and MIM steel grades. Therefore, it does not describe the micro-hardness H_0 of the metallic matrix solely.

As a consequence, the micro-hardness H_0 (metallic matrix hardness), e.g. the HV 0.1 micro-hardness, should be used for the Murakami approach [20]. The second modification is with regard to the effect from the porosity $f=1-\rho/\rho_0$. A. Bergmark [20] had proposed an additional term to reduce the predicted bending fatigue strength at the knee point σ_A value as function of the porosity f. In general, that approach is known as the Balshin equation:

$$P = P_0 \left(\frac{\rho}{\rho_0}\right)^m$$

In this equation, P is a material property, which is affected by the porosity f. P_0 is the fully dense material property (f=0), ρ is the corresponding density, ρ_0 is the full density and m is a characteristic exponent. In the case of Young's modulus E, the Balshin equation is called the MacAdam equation and the characteristic exponent is m=3.4. A Bergmark had applied that term to incorporate the effect (superimposition of the porosity and the single defect) from the porosity f as:

$$\sigma_A = \frac{X(H+120)}{\sqrt[12]{AREA}} \times \frac{E}{E_0} = \frac{X(H+120)}{\sqrt[12]{AREA}} \times \frac{E_0\left(\frac{\rho}{\rho_0}\right)^m}{E_0} = \frac{X(H+120)}{\sqrt[12]{AREA}} \times \left(\frac{\rho}{\rho_0}\right)^m$$

However, this seems to be valid with one exception. The corresponding Balshin exponent must be set as m≈5 since the Balshin exponent of m=3.4 is only valid for the evolution of Young's modulus E. Further research had shown that a Balshin exponent of m≈5 is more typical for cyclic fatigue properties. With the two mentioned modifications, the Murakami approach should be able to predict the bending fatigue strength at the knee point σ_A of sintered and porous PM and MIM steel grades. As illustrated in Fig. 13, it must be understood as a superimposition of the bending fatigue strength at the knee point σ_A of a fully dense material with a single defect, together with a porous material without a defect. For a calibration of the Murakami prediction model, the projected defect area $(AREA)^{0.5}$ in the first principal direction should be varied as long as the experimentally

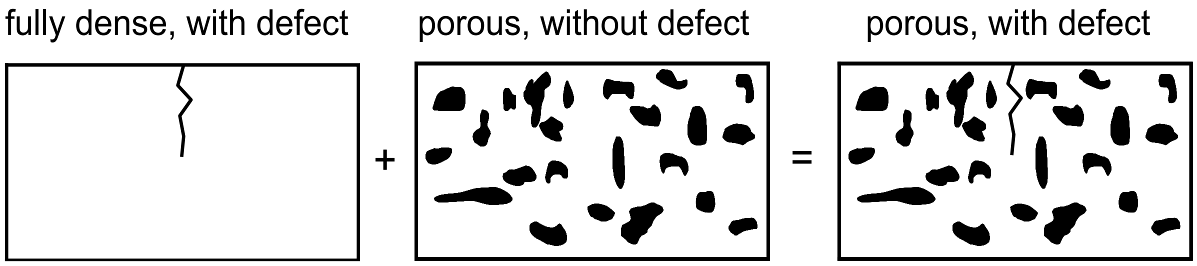

Fig. 13 Superimposition of a fully dense material with a single defect (Murakami approach) together with a porous material without a defect (Balshin approach)

derived bending fatigue strength at the knee point σ_A values are correctly approximated. If a surface defect (X=1.43) is assumed to be critical, a spherical defect with a diameter of d=a≈44 µm (MIM 8620 case-hardened, H_0=667 HV 0.1) or d=a≈51 µm (MIM 100Cr6 hardened, H_0=705 HV 0.1) must be assumed to match the experimental values from Table 2 and Table 3 (1 gate). This first estimation neglects the effect of the porosity f (Balshin equation). In other words, here it was assumed that the defect d=a dominates the material and porosity behaviour. The final calibration of the Murakami prediction model requires the adjustment of both influencing factors (defect size effect according Murakami and porosity effect according Balshin). In practise, a clear differentiation between 'defect' and 'pore of the porosity population' will be difficult due to the wide and skewed probability density distribution of the pore size.

Those predicted defect diameters d=a are in a reasonable range for the two tested MIM steel grades with a sintered density of ρ=7.4 g/cm³. The maximum Feret diameters $d_{max.\ Feret}$ were measured using optical image analysis software for all four specimen geometries, gate variants and for both MIM steel grades as metrics for the largest defect size (without a further differentiation between surface and internal defects). They vary between $d_{max.\ Feret}$=13 µm and $d_{max.\ Feret}$=46 µm. However, the mean value (averaged over all variants) is $d_{max.\ Feret}$=26 µm. This value is approximately half of the predicted spherical defect diameter d=a. After a proper calibration, the Murakami prediction model can be used for further estimations. The Murakami approach also exhibits a mean stress correction term. After our experiences this mean stress correction term is too optimistic. Therefore, the derived mean stress sensitivities M according to the FKM guideline are more representative.

Conclusions

A systematic analysis of twenty in-house derived bending s-N lines of MIM 8620 case-hardened and MIM 100Cr6 hardened materials was undertaken to investigate the pure material behaviour as well as the effect of weld lines and notches.

- The filling and the formation of weld lines were numerically investigated with Mould Flow simulations.
- A twin-gated cavity was designed and built to shift the weld line into the notch root of unnotched and notched fatigue specimens according to DIN EN ISO 3928 with different notch radii r (r=30 mm, r=0.9 mm and r=0.45 mm) to investigate the interface strength.
- A sintered density of ρ=7.4 g/cm³ was achieved for all four specimen geometries and for both MIM steel grades.
- A case-hardening depth of CHD_{550}=0.3 mm was achieved on MIM 8620 case-hardened (measured on the unnotched specimen with the waist radius of r=30 mm) which agrees with the requirements. The surface micro-hardness was estimated as H_0=667 HV 0.1 and the core micro-hardness as H_∞=265 HV 0.1, respectively.
- MIM 100Cr6 hardened was through-hardened to a constant micro-hardness of H_0=H_∞=705 HV 0.1=const.
- Moreover, the macro-hardness H values are comparable (H=631 HV 30 for MIM 8620 case-hardened vs H=626 HV 30 for MIM 100Cr6 hardened). This indicates comparable surface carbon contents C_0 , because the maximum achievable surface hardness H_{max} (hardenability) depends only on the surface carbon content C_0 (and in the case of porous MIM and PM steel grades on the sintered density ρ).
- A systematic trend regarding the weld line position (single-gated vs twin-gated) tensile test specimens on the static tensile test results cannot be found. Differences between the two benchmarked MIM steel grades occur in the case of notches or other stress concentrations. The notch-strength ratios γ of MIM 8620 case-hardened are much better.
- Four complete Haigh diagrams (two MIM steel grades and two gate variants) and the corresponding Haigh damage lines were derived for the fatigue assessment and the fatigue lifetime prediction. The mean stress sensitivities M_2 and M_3 are high and all above $M_{2/3}$=0.52, due to the case-hardened or hardened surface condition.
- The unnotched Haigh damage lines of the two benchmarked

MIM steel grades are very similar. This means that the unnotched bending fatigue strength at the knee point σ_A values are comparable. This statement holds true for all of the three tested loading ratios R (R=-1, R=0 and R=0.5).

- Huge differences occur if notches are present. Similar to the static notch-strength ratios γ (axial loading mode), the cyclic notch factors K_f (bending loading mode) are much better for MIM 8620 case-hardened. Contrary to expectations, MIM 8620 case-hardened is not perfectly notch sensitive, possibly because of the multilayer material structure (hard surface and soft core). This is remarkable because both surface micro-hardness H_0 values are comparable (H_0=667 HV 0.1 for MIM 8620 case-hardened vs H_0=705 HV 0.1 for MIM 100Cr6 hardened).
- Both MIM steel grades discussed are typically chosen for rolling contact fatigue and wear applications (Hertzian pressure loading mode/bearing applications). Those loading modes were not tested in this study. Therefore, there is an uncertainty as to how the tested bending loading mode correlates with the Hertzian pressure loading mode.
- An extension of the classical fatigue strength prediction was presented to incorporate the effect of a single defect. After a calibration, the Murakami approach can be used to predict the bending fatigue strength at the knee point σ_A as a function of the micro-hardness H_0 and the projected defect area $(AREA)^{0.5}$ in the first principal direction.

> *"A clear and very strong advantage arises for MIM 8620 case-hardened in the presence of notches or other stress concentrations. In this case, and which is always the case for mechanical engineering components, MIM 8620 case-hardened exhibits much higher static and cyclic material properties."*

Due to their low and comparable alloying element contents of Cr+Ni+Mo=1.2% for the MIM 8620 material and of Cr+Ni+Mo=1.5% for the MIM 100Cr6 material, the raw material (feedstock) prices are almost comparable. A difference in the production costs can be allocated to the different heat treatment strategies. The carburisation step during the case-hardening of the MIM 8620 material requires some extra time and a better controlled carburising atmosphere. As a rule of thumb, the heat treatment costs per kilogram for a case-hardening treatment are three times those for a more traditional hardening treatment. However, typical MIM components are small and low weight. Therefore, the additional costs for a case-hardening treatment will be a few euro cents more (the cost structure in general depends strongly on the component quantities to be produced and to be treated).

In essence, it can be summarised that both MIM steel grades (MIM 8620 case-hardened vs MIM 100Cr6 hardened) are very similar in the unnotched condition. A clear and very strong advantage arises for MIM 8620 case-hardened in the presence of notches or other stress concentrations. In this case, and which is always the case for mechanical engineering components, MIM 8620 case-hardened exhibits much higher static and cyclic material properties. Therefore, the usage of MIM 8620 case-hardened is to be favoured against the usage of MIM 100Cr6 hardened.

Moreover, a clear HCF domain cannot be recognised for MIM 100Cr6 hardened. Therefore, MIM components made of MIM 100Cr6 hardened should be designed for LLF loadings only. The reliability of each MIM component will be enhanced from these findings, if the additional costs for a case-hardening treatment are accepted. The derived results must be examined carefully if the MIM component is subjected to rolling contact fatigue and wear.

Further static and fatigue experiments are planned for 2021 with MIM 17-4PH precipitation hardened and MIM 8740 hardened steels.

Authors

Dr.-Ing. Markus Schneider
GKN Sinter Metals Engineering GmbH
Radevormwald
Germany
Markus.Schneider@gknpm.com
www.gknpm.com

M.Sc Dennis Wawoczny, GKN Sinter Metals Engineering GmbH, Radevormwald, Germany

Dipl.-Ing. Johannes Bergfeld, Dr.-Ing. Jack Schwarz and B.Sc. Christian Simon
GKN Sinter Metals GmbH
Bad Langensalza
Germany

References

[1] Team of authors: Introduction to Metal Injection Moulding – A Manufacturing Process for Precision Engineering Components, EPMA Shrewsbury, 4th Edition 2019

[2] Autodesk.Help: Bindenähte und verwischte Bindenähte, Fehlerbehebung: Mould Flow Adviser 02 April 2015; https://knowledge.autodesk.com/de/support/mouldflow-adviser?sort=score

[3] Menges, G., Mohren, P.: Anleitung zum Bau von Spritzgießwerkzeugen, Hanser Verlag München Wien, 3rd Edition, 1991

[4] Mannschatz, A., Ahlhelm, M., Moritz, T., Michaelis, A.: 3D visualisation of flow patterns in injection moulded ceramic green parts; *Powder Injection Moulding International* 5 (2011), p. 60-65

[5] Schlieper, G., Dowson, G., Williams, B., Petzoldt, F.: METAL INJECTION MOULDING; European Powder Metallurgy Association, Shrewsbury, 3rd Edition, 2013

[6] German, R. M., Bose, A.: Injection Moulding of Metals and Ceramics; Metal Powder Industries Federation, Princeton, 1st Edition, 1997

[7] German, R. M.: Metal Injection Moulding – A Comprehensive MIM Design Guide, Metal Powder Industries Federation, Princeton, New Jersey, 1st Edition, 2011

[8] German, R. M.: Understanding defects in Powder Injection Moulding: Causes and corrective actions, *PIM International*, Vol. 6, No. 1, p. 33-44, 2012

[9] German, R. M.: Powder Injection Moulding – Design and Applications, Innovative Materials Solutions Inc., State College, PA, 1st Edition, 2003

[10] BASF: Catamold 8620; Processing Instructions, 2006

[11] Schneider, M.: Notch Strength and Sensitivity of Sintered Steels; Proc. Euro PM 2013 Göteborg, Vol. 3, p. 403-408; EPMA, Shrewsbury, 2019

[12] Schneider, M., Kotthoff, G.: Einfluss der Nachbehandlung auf die Schwingfestigkeit von Sinterstählen – Theorie und praktische Anwendung; Prozesswärme-Tagung HärtereiPraxis, p. 93-104; Vulkan-Verlag, Essen, 2018

[13] Schneider, M., Bergfeld, J., Simon, C.: Weld Lines And Its Effect On The Fatigue Response Of Case-Hardened MIM 8620 Steel; Proc. Euro PM 2019 Maastricht, Proc. USB, No. 4349225; EPMA, Shrewsbury, 2019

[14] Schneider, M., Savu, V.-A.: The Support Effect and its Impact on the Design of Complex Shaped Sintered PM Parts; *International Journal of Powder Metallurgy*, Vol. 55, No. 4 (2019), p. 11-22

[15] Schneider, M.: A Safety Factor For Sintered PM Components; Proc. Euro PM 2018 Bilbao, Proc. USB, No. 3984306; EPMA, Shrewsbury, 2018

[16] Burkamp, K., Broeckmann, C., Beiss, P.: Statistical Evaluation and Scatter of Fatigue Strength Data of Sintered Steels; Proc. Euro PM 2019 Masstricht, Proc. USB, No. 4348146; EPMA, Shrewsbury, 2019

[17] Rennert, R., Kullig, E., Vormwald, M., Esderts, A., Siegele, D.: RECHNERISCHER FESTIGKEITSNACHWEIS FÜR MASCHINENBAUTEILE; VDMA Verlag, Frankfurt am Main, 6. Auflage, 2012

[18] Murakami, Y.: Metal Fatigue: Effects of Small Defects and Nonmetallic Inclusions, Elsevier, Amsterdam, 1st Edition, 2002

[19] Klocke, F., Brecher, C.: Zahnrad- und Getriebetechnik, Hanser, München, 1st Edition, 2017

[20] Berkmark, A.: Influence Of Maximum Pore Size on the Fatigue Performance of PM Steel, DF PM 2005, Stara Lesna, p. 1-7